Am J Cancer Res 2026;16(7):2873-2884
www.ajcr.us /ISSN:2156-6976/ajcr0171766

Original Article

Raman microspectroscopy for cervical cancer diagnosis: an ex-vivo cryopreserved tissue analysis

Mariana V Tavares[1,2,3*], Maria M Félix[1,3*], Ana LM Batista de Carvalho[1], Inês P Santos[1], Maria F Botelho[4,5], Luís AE Batista de Carvalho[1], Maria PM Marques[1,6]

[1]Molecular Physical-Chemistry, LAQV/Requimte, Department of Chemistry, University of Coimbra, 3004-535 Coimbra, Portugal; [2]Department of Gynaecology, Portuguese Oncology Institute of Porto, 4200-072 Porto, Portugal; [3]Faculty of Medicine, University of Coimbra, Azinhaga de Santa Comba, Pólo III - Pólo das Ciências da Saúde, 3000-548 Coimbra, Portugal; [4]Coimbra Institute for Clinical and Biomedical Research (iCBR), Area of Environment Genetics and Oncobiology (CIMAGO), Institute of Biophysics, Faculty of Medicine, University of Coimbra, Azinhaga de Santa Comba, Pólo III - Pólo das Ciências da Saúde, 3000-548 Coimbra, Portugal; [5]Center for Innovative Biomedicine and Biotechnology (CIBB), University of Coimbra, Rua Larga, 3004-504 Coimbra, Portugal; [6]Department of Life Sciences, Faculty of Science and Technology, University of Coimbra, 3000-456 Coimbra, Portugal. [*]Equal contributors.

Received January 29, 2026; Accepted June 11, 2026; Epub July 15, 2026; Published July 30, 2026

Abstract: Cervical cancer was the fourth most common cancer worldwide in 2022. There is an urgent clinical need for new objective and reproductible methods aiming an early diagnosis. The aim of the present study is to characterize fresh cryopreserved human cervical tissue through Raman microspectroscopy to identify spectral biomarkers that highlight the chemical differences between healthy and malignant tissues. Normal and tumoral human cervical tissues samples were collected prospectively from patients and from pathology specimens and cryopreserved at -80 °C without any treatment or cryoprotectant. Two parallel 10 µm sections were cut from each tissue block for histopathology and spectroscopy analysis. Raman microspectroscopy using a 532 nm laser was performed in the first minutes after defrosting the sample. Concerning the high-wavenumber region (2800-3600 cm^{-1}) the signals from lipids and proteins are those that most contribute to the spectra of the tumoral samples. In the fingerprint region (600-1800 cm^{-1}) the spectra of the malignant samples show characteristic nucleic acids signals and absence of features from either collagen or glycogen, which are usually present in healthy tissues. Distinct vibrational spectroscopic differences were obtained, and these signals may be considered as spectral biomarkers of tumoral tissues. A successful classification model was constructed to categorize the samples into either healthy or tumoral, with an accuracy higher than 90%. This report evidences the feasibility of Raman microspectroscopy as a reliable and non-invasive diagnostic tool for differentiating healthy from tumoral tissues with high accuracy. The use of snap-frozen tissue samples allows the translation to real-time in vivo fresh samples. Coupled to existing histopathological methods, this technique can is therefore a useful tool in the clinical field for early cancer diagnosis.

Keywords: Cervical cancer, Raman spectroscopy, early diagnosis

Introduction

Cervical cancer is the most common gynaecological malignancy worldwide and the fourth most frequent cancer among women, following breast, lung and colorectal cancers. In 2022, 662.301 new cases of cervical cancer were identified. Since this cancer mainly occurs due to the infection of types 16 and 18 of human papillomavirus (HPV), its incidence varies greatly around the globe. Only 11.8% of cases are expected to occur in high-income countries, reflecting disparities in access to vaccination and screening rather than differences in HPV prevalence [1].

The causal association between persistent HPV infection and cervical carcinogenesis is well established [2, 3]. The onset of high-grade lesions and carcinoma from HPV persistent infection is very slow and takes several years (typically 10 to 20). This slow progression to cancer provides an opportunity for screening and early intervention. Early detection of pre-

https://doi.org/10.62347/KCBL4300

malignant lesions is crucial to prevent progression to invasive disease, making cervical cancer one of the most preventable malignancies when adequate screening is available [3, 4].

Despite organized screening programs across Europe, cervical cancer is the second most deadly cancer in people aged 15 to 64, after breast cancer, highlighting its serious public health impact [1]. The World Health Organization (WHO) has raised global awareness by launching the Cervical Cancer Elimination Initiative Program, focusing on HPV vaccination, screening, and treatment [4].

Current approaches to cervical cancer prevention encompasses both screening and diagnostic modalities. Primary screening methods include cervical cytology (Papanicolaou smear) and HPV testing, while colposcopy with directed biopsy serves as a diagnostic procedure for evaluating abnormal screening results. Cytology-based screening programs have substantially reduced the rates of cervical cancer incidence and mortality over the past five decades [5]. Papanicolaou initially introduced cervical cytology with morphological classifications based on the like hood of leading to cancer. However, the current cytology classification for reporting cervical and vaginal cytology diagnosis - The Bethesda System for Reporting Cervical Cytology - incorporates a view of cervical carcinogenesis that is explicitly based on the natural history of HPV [6]. Despite improvements in the Bethesda system, the Pap smear is still subjective, with a sensitivity around 74% and a specificity of 95-98% [6, 7].

Randomized controlled studies have shown that HPV-based screening offers superior sensitivity for detecting high-grade lesions compared with cytology alone, albeit with lower specificity [8-12]. Current guidelines from the WHO and other international organizations now recommend HPV testing as the preferred primary screening modality in many settings.

Colposcopy remains a critical diagnostic step following abnormal screening results. The procedure involves visual assessment of the cervix after application of acetic acid and iodine solution, with characteristic acetowhite changes and vascular patterns guiding biopsy site selection for histopathological confirmation. However, its effectiveness is limited by intra- and interobserver variability [13, 14]. Therefore, improving diagnostic accuracy through spectroscopic methods has become a key area of research [14]. Regarding cervical cancer screening and diagnosis, the main concerns are efficiency and accuracy.

Research in optical techniques for medical diagnostics has been significantly improved in recent years [15, 16]. Among these, Raman spectroscopy has gained increasing recognition as a promising biomedical tool [15, 17] due to its high analytical accuracy, with specificity ranging from 66-100% and sensitivity from 73-100% [15, 17-19]. This technique is based in inelastic light scattering: when a sample is illuminated by a monochromatic laser radiation, interactions between the incident photons and the molecular vibrations produced scattered light with altered energy corresponding to specific vibrational modes. As a result, the frequencies, relative intensities and shapes of the Raman signals provide in-depth information on the molecular composition of the samples, as well as on its structure and conformational preferences. Biological tissues contain multiple biochemical components - including nucleic acids, proteins, lipids, and carbohydrates - and the corresponding Raman spectrum is the sum of the signals from each individual biochemical component. Thus, a Raman spectrum provides a biochemical fingerprint of the sample [18]. This technique, that evaluates the molecular composition and the biochemical patterns, has demonstrated advantages over current methods for the earlier diagnosis of these alterations in face of the histopathologically detected morphological changes [17-21]. Raman spectroscopy has been used with promising results both ex-vivo and in-vivo/in situ for cervical tissue characterization [22, 23].

The aim of the present study is to characterize fresh cryopreserved human cervical tissue using Raman microspectroscopy. We seek to identify spectral biomarkers that highlight the chemical differences between healthy and malignant tissues, employing cross-validation to assess classification performance.

Methods

Sample collection and preparation for Raman measurements

The cervical tissue samples used in this study were obtained from the Portuguese Institute of

Table 1. Patient characteristics at the time of the cervical biopsies

Variable	Healthy (n=42)	SCC (n=20)
Age (y)		
Median (range)	60.5 (41-88)	57.1 (38-83)
Race		
Causasian	42	18
Black	0	2
Menarche age (y)	12.8 (11-16)	12.6 (9-17)
Sexually active		
Yes	38	20
No	4	0
Nuliparous	10	2
Multiparous	32	18
Menopause age (y)	50.6 (45-56)	52 (28-55)
Cervical cytology		
Normal	40	0
HSIL	N/A	4
SCC	N/A	7
Unkown	2	9
Cervical lesion	N/A	
Ulcera	N/A	9
Exofitic lesion	N/A	11

HSIL, high-grade intraepithelial lesion; SCC, squamous cell carcinoma.

Oncology of Porto (IPO-Porto) with previous patient consent and approval from the hospital's Ethical Committee (CES 264/020). Forty-two samples from healthy cervical tissue were obtained from surgical specimens after hysterectomy due to a gynaecological-related tumour or for prophylactic intent in patients with an increased risk for gynaecological tumours by risk mutation (Lynch syndrome and others). The normal histopathology of the cervical tissue was confirmed by a pathologist dedicated to gynaecology.

The study group was comprised of twenty squamous cervical cancer (SCC) samples collected directly from cervical biopsy from 20 patients with clinical macroscopic cervical tumours, at IPO-Porto gynaecology outpatient clinic from May 2022 to May 2023. **Table 1** summarizes the patient's characteristics. No formal statistical comparisons were performed. Overall, the groups showed similiar distributions in terms of race, median aged of menarche, menopause and parity. Only squamous cervical tumours were analysed, cervical adenocarcinoma and other tumour histologies being excluded, as biochemical composition varies according to the histopathological type of epithelial cervical cancer [24]. Indeed, if the aforementioned exclusion had not been carried out, the observed discrimination might have resulted from differences in the composition between tumor types rather than between healthy and malignant tissues, which is the intended comparison in this study.

All samples were cryopreserved at -80°C, without any treatment or cryoprotectant. Two parallel 10 μm sections were cut from each tissue block, using a cryomicrotome, and were mounted on glass slides. One section from each sample was stained with haematoxylin and eosin, for histopathological purposes and the other slide was used to perform spectroscopic analysis. Although standard histological sections are routinely cut at a thickness of approximately 4 μm, in this study 10 μm sections were prepared to enable an effective acquisition of Raman spectra. This decision was made at the initial stage of the project, balancing the optical requirements of Raman spectroscopy with the need to preserve sufficient histological detail for microscopic analysis. Thicker sections (10 μm) allowed for improved signal-to-noise ratio in spectroscopic measurements, without significantly compromising the morphological assessment of the tissue. These samples were cryopreserved and transported in dry ice to the Molecular Physical-Chemistry R&D Unit, at the University of Coimbra (QFM-UC), for spectroscopic analysis. The samples were taken off the freezer, and the spectra were measured immediately (in the first minutes after defrosting).

Raman instrumentation and spectral acquisition

The acquisition of microRaman spectra was performed in an Oxford Instruments WITec (Ulm, Germany) confocal Raman microscope system alpha300R (using a 100×/0.8 Zeiss Epiplan objective, estimated Airy Disc Diameter of 0.81 μm) coupled to an ultra-high-throughput spectrometer (UHTS) 300 VIS-NIR equipped with a thermoelectrically refrigerated (-55°C) front-illuminated charged-coupled device detector (CDD). A 532 nm diode-pumped solid-state laser based on frequency doubled Nd:YAG was used as exciting radiation. The laser incidence power on the sample was kept at 11 mW and each spectrum were obtained with 5 accumulations of 5 seconds (i.e. in total 25 s), for both healthy and tumoral specimens.

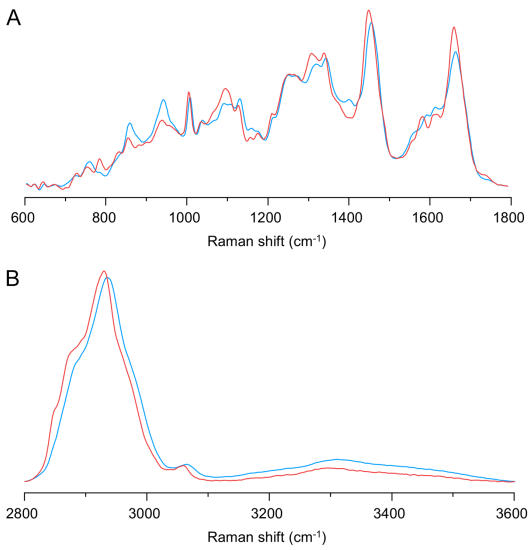

Figure 1. Average Raman spectra of healthy and tumoral (SCC) samples in the fingerprint (A) and high wavenumber regions (B). Blue - Healthy; Red - SCC.

Data analysis

Prior to any data analysis, the Raman spectra were initially cropped to the pre-processing spectral range (400-3600 cm^{-1}). A principal component (PC)-based noise reduction algorithm was applied by retaining a selected number of principal components (25 PC's) and then recombining the dataset. All spectra were further cropped into two spectral regions: fingerprint region (400-1800 cm^{-1}) and high-wavenumber region (2800-3800 cm^{-1}). The spectra were baseline corrected (1^{st} order polynomial), and vector normalized. These analyses were performed using MATLAB_R2023b (MathWorks, USA).

Unsupervised Principal Component Analysis (PCA) was carried out with standard singular value decomposition of the data, using Quasar Spectroscopy 1.11 software [25]. The order of the principal components (PC) denotes their importance in relation to the data set variance, PC1 corresponding to the highest variance present in the data.

Data classification was performed using the MATLAB R2023b (machine learning toolbox). The classification model was a Principal Component Analysis - Linear Discriminant Analysis (PCA-LDA) with linear kernel function. The model accuracy was assessed by computing the sensitivity, specificity, and area under the curve (AUC) of the receiver operating characteristics (ROC) curves. The diagnosis capability of the model was evaluated using confusion matrices.

To validate the PCA-LDA model created, an independent validation test using 9 SCC samples from patients not included in model development dataset (149 spectra) was performed.

Results

Figure 1 shows the mean Raman spectra for healthy (767 spectra) vs. tumoral (613 spectra) samples concerning fingerprint (**Figure 1A**) and high-wavenumber region (**Figure 1B**), respectively, and the corresponding assignments are comprised in **Table 2**. The frequency values and intensities of the Raman signals allow to obtain information regarding the samples. Clear spectral differences and biocehmical fingerprints are observed in healthy and SCC tissues. The most important bands in tumoral samples are due to DNA and RNA, amino acids and proteins. Concerning healthy samples, the most prominent signals are from collagen, glycogen, lipids and amino acids.

In order to retrieve the maximum information embedded in the spectra, multivariate analysis was applied to identify the most significant differences between groups (healthy and tumoral samples). A PCA analysis allows to reduce the dimensionality of the dataset and to differentiate between healthy and tumoral tissue samples. PC3, explaining 19.3% of the total data variance, was considered the principal component that best discriminates tumoral from normal samples in the fingerprint region (**Figure 2A**), while PC1 explains 75.8%, for the high-wavenumber region (**Figure 2B**).

When analysing the fingerprint region (**Figure 2A**), the bands of nucleic acids (782, 1089 cm^{-1}), amino acids (1000 and 1332 cm^{-1}, phenylalanine and tryptophane), RNA and DNA (1204, 1301 and 1574 cm^{-1}) and proteins (1653 cm^{-1}) are the features that most contribute to spectra of the tumoral samples. On the other hand, in normal samples, the major signals correspond to amino acids (858 cm^{-1}), glycogen (938 cm^{-1}), collagen (1035, 1242 cm^{-1}) and phospholipids and lipid membranes (1273 and 1395 cm^{-1}). Concerning the high-wavenumber region (**Figure 2B**), the bands at 2847 and 2868 cm^{-1} for CH_2 and CH_3 symmetric stretching for lipids and proteins are the

Table 2. Raman wavenumbers and assignment for cryopreserved healthy and tumoral human cervical tissue

Wavenumber (cm^{-1})	Nucleic acids	Proteins	Lipids	Carbohydrates	References
621		Phe(t(CC))			[35-37]
642-645		ν(CS), Tyr(t(CC))			[36, 37]
670	β-DNA/G,T($\nu_S(CC)_{ring}$)				[35, 37]
671		Trp ($\nu_S(CC)_{ring}$)			[37]
722	($\nu_S(CC)_{ring}$)β-DNA/A	($\nu_S(CC)_{ring}$)$_{Trp}$			[38]
724-725	Ac nucleic (DNA/RNA bases ring breathing)				[36, 37]
750	Z-DNA ($\nu(OPO)_{backbone}$)	Trp ($\nu_s(CC)_{ring}$)			[35]
756	β-DNA/dT ($\nu CC)_{ring}$)	Trp ($\nu_s(CC)_{ring}$)			[35, 38]
782-783	C,T,U ($\nu(CC)_{ring}$)				[36, 37]
829-830	β-DNA ($\nu(OPO)_{backbone}$)	Pro,Tyr (ν(CC))			[35, 37]
852-853		$\nu(CC)_{Pro,Tyr,Val}$		$\gamma(COC)_{polysaccharides}$	[36, 37]
856		Pro,Tyr, Val (ν(CC), δ(CCH))		$\gamma(COC)_{polysaccharides}$	[35-37]
879	RNA ribose ($\nu(CC)_{ring}$)	Pro, Hyp, Tyr, Collagen ($\nu(OPO)_{backbone}$)	Phosphocoline ($V_S(CCN^+)$	ν(CC), ($\nu(CO)_{ring}$)	[35-38]
898		ρ(CH_2)		Monosacharides(β-glucose), (C-O-C) skeletal; Disaccharide (maltose)	[35-38]
937-939		Pro ($\nu(CC))_{backbone}$	Glçycolipids (ν(COC)	(ν(COC)	[36]
954		Phosphorylated proteins (ν(OPO))			[37]
1002-1003		Phe ($\nu_S(CC)_{ring}$			[35-37]
1032		Phe (δ(CH)), ν(O-CH_3)	ν(CC), Phospholipids (δ(CH))	ν(CC), ν(CO), ν(C-OH)	[35-37]
1035		Collagen			[36, 37]
1062-1063	βDNA/deoxyribose (ν(CO))	ν(CC), ν(CN)	ν(CC), ν(CO)	ν(CC), ν(CO), δ(OCH)	[35, 38]
1084	$\nu_s(PO_2^-)_{B\text{-}DNA}$	ν(CN)			[38, 39]
1088-1089	PO_2^- stretching			C-C stretch	[36, 37]
1092	$\nu_s(PO_2^-)_{B\text{-}DNA}$				[26, 36, 37]
1105-1106				Carbohydrates	[36, 40]
1123		ν(CN)	$\nu(CC)_{acyl(trans\ conoformation)}$	ν(CO), ν(CC)	[26, 36, 38]
1126	RNA/ribose (ν(CO))	ν(CN)	$\nu(CC)_{acyl(trans\ conoformation)}$	ν(CO), ν(CC)	[35, 36]
1155		ν(CN), ν(CN)		Glycogen	[36]
1157		ν(CN), ν(CN), ρ(CH_2)	ρ(CH_2), ν(=C-C=)$_{conjugated}$	ρ(CH_2)	[35, 36, 38]
1171-1172	($\nu(CC)_{ring}$)$_{C,G,T}$	Tyr (δ(CH))			[26, 37]
1207-8	DNA/RNA bases (A,T)	Tyr, Phe, Hyp (ν(CC))		Amide III	[35-37]
1210		Tyr, Phe (ν(C-C_6H_5)) mode			[36, 37, 40]
1244?		Amide III/random coil			[35]
1247-1248	Guanine, cytosine (NH_2)	Amide III/collagen			[36, 37]
1261	A,T ($\nu(CC)_{ring}$)	δ(CH_2), δ(C=C-H)	δ(CH_2), δ(C=CH)$_{phospholip}$	δ(CH_2), w(CH_2), t(CH_2)	[35]

1270	RNA/C,U ($\nu(CC)_{ring}$)		Phospholipids ($\delta(C=C)$		[35]
1304	($\nu(CC)_{ring}$)RNA, A,C		CH_2 deformation		[26, 36, 37]
1316	G ($\nu(CC)_{ring}$)				[36, 37]
1335	CH_2CH_3 wagging & twisting mode in collagen, nucleic acid & tryptophan				[36, 37]
1341	A,G ($\nu(CC)_{ring}$)	$\delta(CH_2)$, Trp($\nu(CC)_{ring}$)		$\delta(CH_2)$	[35]
1372	A,G,T ($\nu(CC)_{ring}$)				[36, 41]
1396		$\delta(CH_2)$, $\rho(CH_2)$	Membrane lipids ($\delta(CH_2)$	$\delta(CH_2)$, $\rho(CH_2)$	[26, 35]
1399		$t(NH_2)$			[36-38]
1445			$\delta(CH_2)$		[35, 37, 38]
1452		CH_2, CH_3 deform. (collagen)			[36, 37]
1510		Tyr ($\nu(CC)_{ring}$)			[35]
1554		Amide II ($\delta(CNH)$)			[36, 37]
1557	G ($\nu(CC)_{ring}$)	Trp ($\nu(CC)_{ring}$), $\nu(C=C)_{porphyrin}$			[35-37, 39]
1579	A,G ($\nu(CC)_{ring}$)				[35, 40]
1588		Phe, Hyp ($\delta(CC)$)			[36, 37]
1604	T ($\nu(CC)_{ring}$)	Phe ($\delta(C=CH)$)			[35]
1610	C (NH_2)				[36, 37]
1613		Amide I/β-sheet, anti-parallel			[38]
1657		Amide I ($\nu(C=O)$)	$\nu(C=C)$		[36, 37]
1660	DNA ($\delta(NH)$)	Amide I ($\nu(C=O)$)/a-helix	$\nu(C=C)$		[35]
1731-1739			($\nu(C=O)_{ester}$)		[35, 38]
2847		ν_s (CH_2)	ν_s (CH)	ν_s (CH_2)	[26]
2850-2875		ν_s (CH_2)	ν_s (CH), ν_s (CH_2)	ν_s (CH_2)	[35, 36]
2880-2881		ν_s (CH_3)	ν_s (CH_3)	ν_s (CH_3)	[38]
2892		ν_{as} (CH_2)	ν_{as} (CH_2)	ν_{as} (CH_2)	[35]
2930		ν_{as} (CH_2)	ν_{as} (CH_2)	ν_{as} (CH_2)	[38]
2936-37		ν_{as} (CH_2)	ν_{as} (CH_2)	ν_{as} (CH_2)	[38]
2947-2950			ν_{as} (CH_3)		[36, 40]
2987-2988			cholesterol ester		[38]
3060-3065		ν_{as} (CH_2)			[35]
3274		Amide A ($\nu(NH)$)			[35, 38]
3309			ν_{as} (CH)	ν_{as} (CH)	[35, 38]

The vibrational modes shown in black are the most prominent in healthy tissue and those in red are prevalent in tumoral samples. A, Adenine; C, Cytosine; G, Guanine; Hyp, Hydroxyproline; Phe, Phenylalanine; Pro, Proline; T, Thymine; Trp, Tryptophan; Tyr, Tyrosine; U, Uracil; δ, in place-deformation; ν, stretching; t, twisting; ω, wagging; s, symmetric; as, anti-symmetric.

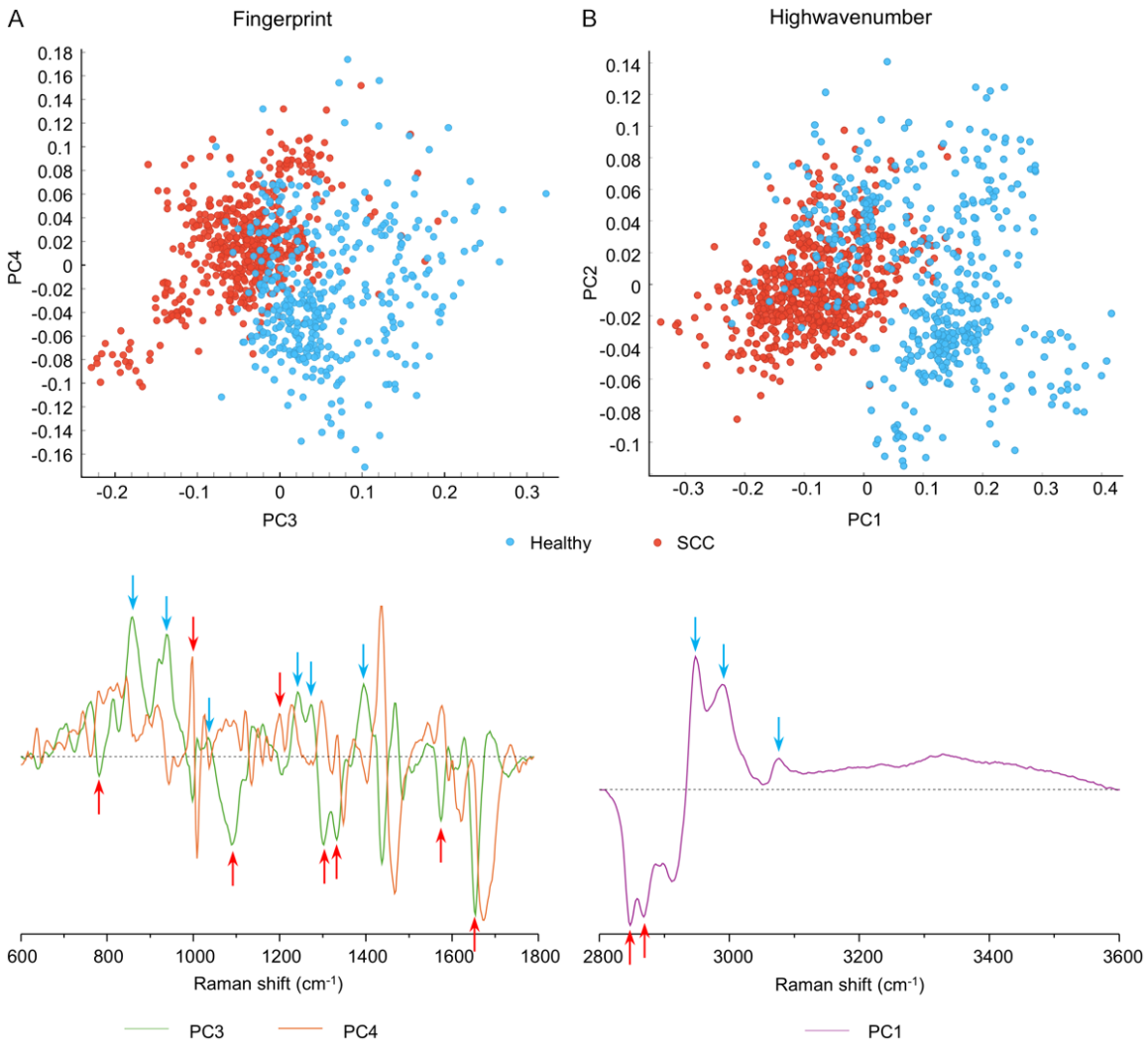

Figure 2. PCA analysis with PC scores with their corresponding loadings for fingerprint (A) and high wavenumber (B) regions. In (A), the scores at the left of zero are tumoral samples Raman spectra and at the right of the zero mostly healthy samples. In (B), wavenumbers whose loadings were above zero contributed majorly to healthy samples and wavenumbers below zero to tumoral samples.

spectral features that most contribute to tumoral samples and could be considered as spectral biomarkers. On the other hand, the bands at 2947 and 2988 cm^{-1} ascribed to the antisymmetric CH_2 stretching and at 3065 cm^{-1} related to the Amide B feature (due to Fermi resonance between the first overtone of Amide II and A) could be considered a spectral marker of normal samples.

In order to develop a classification model, the PCA-LDA classifier was further applied. A cross-validated classification was obtained and compared the Raman microspectroscopy analysis with the histopathological gold standard. **Figure 3A** and **Figure 3B** illustrate the receiver operating characteristics (ROC) curves generated for fingerprint and high-wavenumber regions, respectively. The areas under the ROC curves (AUC) were 0.96 for the fingerprint region (95% CI: 0.949-0.971), with 95.0% sensitivity (confidence interval 95% (CI): 93.4-96.6%), 89.1% specificity (CI 95%: 86.7-91.5%) and 92.0% overall accuracy (CI 95%: 90.9-92.3%), and 0.92 for the high wavenumber region (95% CI: 0.904-0.936), with 69.5% sensitivity (CI 95%: 66.7-72.3%), 73.0% specificity (CI 95%: 69.5-72.5%) and 70.8% overall accuracy (CI 95%: 68.6-73%).

An independent test was performed to validate the PCA-LDA model created (training model).

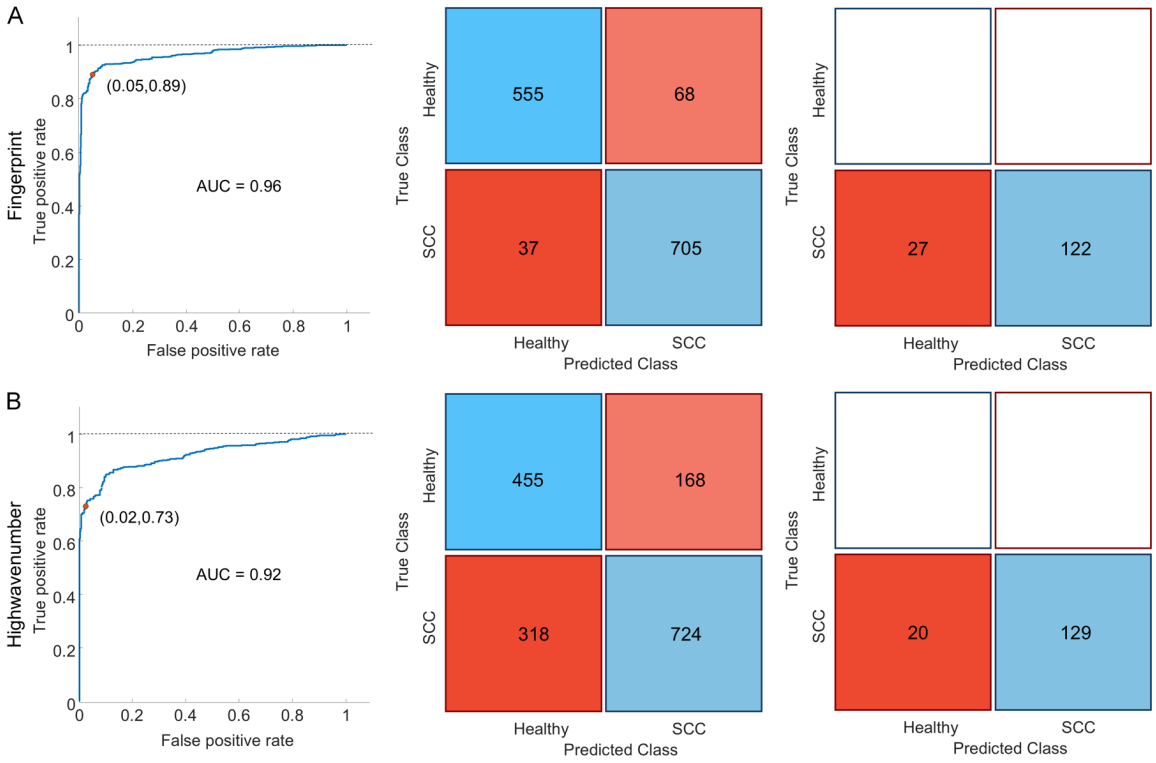

Figure 3. Raman model performance for fingerprint (A) and high wavenumber (B) regions. The ROC curve (left panel) and confusion matrices of the model tumoral vs. normal (middle panel) are represented as well as confusion matrixes for the independent validation test on SCC samples (right panel).

Nine tumoral samples (149 spectra) who were not included in the model development were analysed. Cross-validation classification results showed sensitivity of 81.9% for the fingerprint region, with 122 correct matches (true positives) and 27 incorrect matches (false negatives). For the high-wavenumber region, a sensitivity of 86.6% was achieved, with 129 true positive matches.

Discussion

The present study demonstrates that Raman microspectroscopy can accurately discriminate healthy from invasive cervical squamous cell carcinoma using cryopreserved human tissue.

The spectra of tumoral samples (as described earlier) exhibited prominent nucleic acids bands at 782, 1089, 1204, 1301 and 1574 cm^{-1}, alongside elevated lipid (2847 cm^{-1}) and Amide I (1653 cm^{-1}) signals. Conversely, bands associated with collagen (1035 cm^{-1}), glycogen (938 cm^{-1}) and Amide III (1242 cm^{-1}) were absent or markedly diminished (**Table 1**).

These spectral changes reflect the biochemical hallmarks of neoplastic transformation. Enhanced nucleic acid signals indicate increased mitotic activity and an elevated nuclear-to-cytoplasm ratio characteristic of proliferating tumour cells [26-28]. The accumulation of cytoplasmic lipid droplets, a recognized feature of malignancy, accounts for the intensified CH_2 stretching bands [29, 30]. Structural proteins such as collagen are present in normal tissues but decrease in tumoral ones mainly due to loss of differentiation during neoplastic progression [27]. The diminished glycogen content in tumoral tissue is due to a loss of cervical epithelial cell maturation caused by defective glycogen synthesis [27]. Notably, glycogen depletion correlates with enhanced production of enzymes (e.g. matrix metalloproteinases) that degrades the basal membrane thus hindering the production of new proteins and further aiding in carcinoma progression [26]. The Amide III signal (1242 cm^{-1}) is present in normal tissue spectra but absent in tumoral spectra. This finding has already been reported in studies using fresh or frozen samples [31]. An increas-

ed intensity of the Amide I band (1653 cm^{-1}) for invasive carcinoma has also been reported [20, 27], as well as for phenylalanine (1000 cm^{-1}) and tryptophane (1332 cm^{-1}) (essential amino acids for protein synthesis), which reveal an enhanced cellular proliferation characteristic of neoplasms.

Concerning the high-wavenumber region, the signals at 2847 and 2868 cm^{-1}, arising from CH_2 symmetric stretching of lipids and proteins, were found predominantly in tumoral samples and may therefore serve as reliable spectral biomarkers. Conversely, the band at 3309 cm^{-1}, assigned to the OH stretching (water content), may be considered a marker of normal tissue [29]. These findings are consistent with those of Duraipandian *et al*. [32], who demonstrated that normal cervical tissue exhibits high intracellular water content, which can vary depending on pre- or postmenopausal status. To our knowledge, the use of water content as a discriminating factor in cervical cancer, has not been previously reported. In other solid tumours, such as oral cancer, high wavenumber Raman spectroscopy has been shown to distinguish oral cavity squamous cell carcinoma from surrounding non-cancerous tissue with 99% sensitivity and 92% specificity based on water concentration [28]. Interestingly, this does not appear to hold for laryngeal cancer, where water concentration was not found to be a discriminating factor [30]. Further investigation is required to establish wether tissue hydration may represent a robust biomarker for cervical diagnosis.

A major strength of this study is the use of cryopreserved human cervical tissue samples (tumoral and healthy) stored at -80°C, which preserves tissues close to their native biochemical state without the need for dyes or chemical preservatives. This approach offers a significant advantage over studies employing fixatives or embedding media, which can alter sample components - particularly protein conformation - and often introduce spectral features that interfere with accurate signal detection. Paraffin, commonly used in histopathological preparation, is particularly problematic as it affects tissue morphology and produce intense CH_2 bands that may obscure endogenous signals, making challenging to draw reliable conclusions [33, 34].

A further strength lies in the spectral range analysed. Unlike most studies focusing exclusively on the fingerprint region [18, 20, 23], this study analyses both fingerprint and high-wavenumber regions, demonstrating that both provide complementary information and enable accurate discrimination between healthy and tumoral tissue. A classification model was developed, confirming the effectiveness of Raman spectroscopy for this diagnostic application.

This study has several limitations that warrant consideration. First, the small sample size, reflecting the limited availability of cervical cancer cases both at our institution and nationally, as well as the analysis was restricted to squamous tumours - although these represent the majority (~70-80%) of cervical malignancies. Second, control tissues were derived from hysterectomy specimens. While histologically confirmed as normal cervical tissue, patients undergoing hysterectomy may present differences in age, hormonal status or variations related to inflammatory processes or subclinical infections. These factors may influence the biochemical composition and microenvironment of the tissues, potentially affecting their Raman spectral profile independently of malignant transformation. These potential biological confounders should be considered when interpreting the results. Moreover, the absence of portable Raman spectrometers for routine use in clinical settings restricts routine clinical applications.

These results mark a significant advancement in cervical cancer diagnosis. Raman microspectroscopy successfully discriminated healthy from tumoral cervical tissue, achieving 95% sensitivity, 89% specificity and 92% overall accuracy in the fingerprint region, and 98% sensitivity, 73% specificity and 86% accuracy in the high-wavenumber region. Clinical translation appears feasible using portable Raman devices operable by non-expert users with user-friendly software for real-time analysis post-biopsy or directly on cervical tissue.

Conclusions

Distinct Raman spectral signatures of patient biopsies have enabled an accurate characterisation of the biochemical changes associated with malignant transformation and allowed to

identify specific spectral biomarkers in both human healthy cervical epithelium and squamous cell carcinoma. Samples were snap-frozen to preserve tissue integrity and minimize spectral artifacts. While these *ex vivo* results are promising, further validation in *in vivo* conditions is essential prior to clinical translation. The classification model currently developed achieved over 90% accuracy in distinguishing healthy from cancerous tissue. These findings support Raman spectroscopy as a highly promising diagnostic tool, improving real-time tissue characterisation alongside traditional histopathology in clinical settings.

Acknowledgements

Mariana V. Tavares acknowledges Portuguese Society of Gynaecology for the 2023 Research Grant award. This work received support from the Portuguese Foundation for Science and Technology (FCT) within the scope of the project UID/50006/2025 - Associated Laboratory for Green Chemistry - Clean Technologies and Processes - LAQV/Requimte (https://doi.org/10.54499/UID/50006/2025), the A.L.M. B.d.C. employment contract (https://doi.org/10.54499/CECIND/00069/2017/CP1460/CT0029) and the M.M.F. PhD Grant (2024.02-780.BD).

Disclosure of conflict of interest

None.

Address correspondence to: Dr. Mariana V Tavares, Department of Gynaecology, Portuguese Oncology Institute of Porto, 4200-072 Porto, Portugal. ORCID: 0000-0002-2502-3597; E-mail: m.vide@hotmail.com

References

[1] Bray F, Laversanne M, Sung H, Ferlay J, Siegel RL, Soerjomataram I and Jemal A. Global cancer statistics 2022: GLOBOCAN estimates of incidence and mortality worldwide for 36 cancers in 185 countries. CA Cancer J Clin 2024; 74: 229-263.

[2] Crosbie EJ, Einstein MH, Franceschi S and Kitchener HC. Human papillomavirus and cervical cancer. Lancet 2013; 382: 889-899.

[3] Walboomers JM, Jacobs MV, Manos MM, Bosch FX, Kummer JA, Shah KV, Snijders PJ, Peto J, Meijer CJ and Muñoz N. Human papillomavirus is a necessary cause of invasive cervical cancer worldwide. J Pathol 1999; 189: 12-19.

[4] Global Strategy to Accelerate the Elimination of Cervical Cancer As a Public Health Problem. Geneva: World Health Organization, 2020.

[5] Gustafsson L, Pontén J, Bergström R and Adami HO. International incidence rates of invasive cervical cancer before cytological screening. Int J Cancer 1997; 71: 159-165.

[6] Schiffman M, Wentzensen N, Wacholder S, Kinney W, Gage JC and Castle PE. Human papillomavirus testing in the prevention of cervical cancer. J Natl Cancer Inst 2011; 103: 368-383.

[7] Kitchener HC, Blanks R, Cubie H, Desai M, Dunn G, Legood R, Gray A, Sadique Z and Moss S; MAVARIC Trial Study Group. MAVARIC - a comparison of automation-assisted and manual cervical screening: a randomised controlled trial. Health Technol Assess 2011; 15: iii-iv, ix-xi, 1-170.

[8] Mayrand MH, Duarte-Franco E, Rodrigues I, Walter SD, Hanley J, Ferenczy A, Ratnam S, Coutlée F and Franco EL; Canadian Cervical Cancer Screening Trial Study Group. Human papillomavirus DNA versus Papanicolaou screening tests for cervical cancer. N Engl J Med 2007; 357: 1579-1588.

[9] Naucler P, Ryd W, Törnberg S, Strand A, Wadell G, Elfgren K, Rådberg T, Strander B, Johansson B, Forslund O, Hansson BG, Rylander E and Dillner J. Human papillomavirus and Papanicolaou tests to screen for cervical cancer. N Engl J Med 2007; 357: 1589-1597.

[10] Bulkmans NW, Berkhof J, Rozendaal L, van Kemenade FJ, Boeke AJ, Bulk S, Voorhorst FJ, Verheijen RH, van Groningen K, Boon ME, Ruitinga W, van Ballegooijen M, Snijders PJ and Meijer CJ. Human papillomavirus DNA testing for the detection of cervical intraepithelial neoplasia grade 3 and cancer: 5-year follow-up of a randomised controlled implementation trial. Lancet 2007; 370: 1764-1772.

[11] Ronco G, Giorgi-Rossi P, Carozzi F, Confortini M, Dalla Palma P, Del Mistro A, Ghiringhello B, Girlando S, Gillio-Tos A, De Marco L, Naldoni C, Pierotti P, Rizzolo R, Schincaglia P, Zorzi M, Zappa M, Segnan N and Cuzick J; New Technologies for Cervical Cancer screening Working Group. Efficacy of human papillomavirus testing for the detection of invasive cervical cancers and cervical intraepithelial neoplasia: a randomised controlled trial. Lancet Oncol 2010; 11: 249-257.

[12] Barroeta JE, Adhikari-Guragain D and Grotkowski CE. Cervical cancer screening in the era of HPV vaccination: a review of shifting paradigms in cytopathology. Diagn Cytopathol 2017; 45: 903-914.

[13] Origoni M, Cantatore F, Sopracordevole F, Clemente N, Spinillo A, Gardella B, De Vincenzo R, Ricci C, Landoni F, Di Meo ML, Ciavattini A, Di Giuseppe J, Preti E, Iacobone AD, Carriero C, Dellino M, Capodanno M, Perino A, Miglioli C, Insolia L, Barbero M and Candiani M. Colposcopy accuracy and diagnostic performance: a quality control and quality assurance survey in Italian tertiary-level teaching and academic institutions-the Italian society of colposcopy and Cervico-vaginal pathology (SICPCV). Diagnostics (Basel) 2023; 13: 1906.

[14] Perkins R, Jeronimo J, Hammer A, Novetsky A, Guido R, Del Pino M, Louwers J, Marcus J, Resende C, Smith K, Egemen D, Befano B, Smith D, Antani S, de Sanjose S and Schiffman M. Comparison of accuracy and reproducibility of colposcopic impression based on a single image versus a two-minute time series of colposcopic images. Gynecol Oncol 2022; 167: 89-95.

[15] Mamede AP, Santos IP, Batista de Carvalho ALM, Figueiredo P, Silva MC, Tavares MV, Marques MPM and Batista de Carvalho LAE. A new look into cancer-a review on the contribution of vibrational spectroscopy on early diagnosis and surgery guidance. Cancers (Basel) 2021; 13: 5336.

[16] Félix MM, Tavares MV, Santos IP, Batista de Carvalho ALM, Batista de Carvalho LAE and Marques MPM. Cervical squamous cell carcinoma diagnosis by FTIR microspectroscopy. Molecules 2024; 29: 922.

[17] Santos IP, Barroso EM, Bakker Schut TC, Caspers PJ, van Lanschot CGF, Choi DH, van der Kamp MF, Smits RWH, van Doorn R, Verdijk RM, Noordhoek Hegt V, von der Thüsen JH, van Deurzen CHM, Koppert LB, van Leenders GJLH, Ewing-Graham PC, van Doorn HC, Dirven CMF, Busstra MB, Hardillo J, Sewnaik A, Ten Hove I, Mast H, Monserez DA, Meeuwis C, Nijsten T, Wolvius EB, Baatenburg de Jong RJ, Puppels GJ and Koljenović S. Raman spectroscopy for cancer detection and cancer surgery guidance: translation to the clinics. Analyst 2017; 142: 3025-3047.

[18] Lyng FM, Traynor D, Ramos IR, Bonnier F and Byrne HJ. Raman spectroscopy for screening and diagnosis of cervical cancer. Anal Bioanal Chem 2015; 407: 8279-8289.

[19] Wang W, Zhao J, Short M and Zeng H. Real-time in vivo cancer diagnosis using Raman spectroscopy. J Biophotonics 2015; 8: 527-545.

[20] Rubina S and Krishna CM. Raman spectroscopy in cervical cancers: an update. J Cancer Res Ther 2015; 11: 10-17.

[21] Duraipandian S, Zheng W, Ng J, Low JJ, Ilancheran A and Huang Z. Near-infrared-excited confocal Raman spectroscopy advances in vivo diagnosis of cervical precancer. J Biomed Opt 2013; 18: 067007.

[22] Shen ZW, Zhang LJ, Shen ZY, Zhang ZF, Xu F, Zhang X, Li R and Xiao Z. Efficacy of Raman spectroscopy in the diagnosis of uterine cervical neoplasms: a meta-analysis. Front Med (Lausanne) 2022; 9: 828346.

[23] Shaikh R, Daniel A and Lyng FM. Raman spectroscopy for early detection of cervical cancer, a global women's health issue-a review. Molecules 2023; 28: 2502.

[24] Zheng C, Qing S, Wang J, Lü G, Li H, Lü X, Ma C, Tang J and Yue X. Diagnosis of cervical squamous cell carcinoma and cervical adenocarcinoma based on Raman spectroscopy and support vector machine. Photodiagnosis Photodyn Ther 2019; 27: 156-161.

[25] Toplak M, Read ST, Sandt C and Borondics F. Quasar: easy machine learning for biospectroscopy. Cells 2021; 10: 2300.

[26] Santos IP, Martins CB, Batista de Carvalho LAE, Marques MPM and Batista de Carvalho ALM. Who's who? Discrimination of human breast cancer cell lines by Raman and FTIR microspectroscopy. Cancers (Basel) 2022; 14: 452.

[27] Lyng FM, Faolain EO, Conroy J, Meade AD, Knief P, Duffy B, Hunter MB, Byrne JM, Kelehan P and Byrne HJ. Vibrational spectroscopy for cervical cancer pathology, from biochemical analysis to diagnostic tool. Exp Mol Pathol 2007; 82: 121-129.

[28] Barroso EM, Smits RW, van Lanschot CG, Caspers PJ, Ten Hove I, Mast H, Sewnaik A, Hardillo JA, Meeuwis CA, Verdijk R, Noordhoek Hegt V, Baatenburg de Jong RJ, Wolvius EB, Bakker Schut TC, Koljenović S and Puppels GJ. Water concentration analysis by Raman spectroscopy to determine the location of the tumor border in oral cancer surgery. Cancer Res 2016; 76: 5945-5953.

[29] Zietkowski D, deSouza NM, Davidson RL and Payne GS. Characterisation of mobile lipid resonances in tissue biopsies from patients with cervical cancer and correlation with cytoplasmic lipid droplets. NMR Biomed 2013; 26: 1096-1102.

[30] van Lanschot C, Schut TB, Barroso E, Sewnaik A, Hardillo J, Monserez D, Meeuwis C, Keereweer S, de Jong RB, Puppels G and Koljenović S. Raman spectroscopy to discriminate laryngeal squamous cell carcinoma from non-cancerous surrounding tissue. Lasers Med Sci 2023; 38: 193.

[31] Kamemoto LE, Misra AK, Sharma SK, Goodman MT, Luk H, Dykes AC and Acosta T. Near-infrared micro-Raman spectroscopy for in vitro detection of cervical cancer. Appl Spectrosc 2010; 64: 255-261.

[32] Duraipandian S, Zheng W, Ng J, Low JJ, Ilancheran A and Huang Z. Non-invasive analysis of hormonal variations and effect of postmenopausal Vagifem treatment on women using in vivo high wavenumber confocal Raman spectroscopy. Analyst 2013; 138: 4120-4128.
[33] Nallala J, Lloyd GR and Stone N. Evaluation of different tissue de-paraffinization procedures for infrared spectral imaging. Analyst 2015; 140: 2369-2375.
[34] Mamede AP, Santos IP, Batista de Carvalho ALM, Figueiredo P, Silva MC, Marques MPM and Batista de Carvalho LAE. Breast cancer or surrounding normal tissue? A successful discrimination by FTIR or Raman microspectroscopy. Analyst 2022; 147: 4919-4932.
[35] Batista de Carvalho AL, Pilling M, Gardner P, Doherty J, Cinque G, Wehbe K, Kelley C, Batista de Carvalho LA and Marques MP. Chemotherapeutic response to cisplatin-like drugs in human breast cancer cells probed by vibrational microspectroscopy. Faraday Discuss 2016; 187: 273-298.
[36] Movasaghi Z, Rehman S and Rehman IU. Raman spectroscopy of biological tissues. Applied Spectroscopy Reviews 2007; 42: 493-541.
[37] Ramos IR, Meade AD, Ibrahim O, Byrne HJ, McMenamin M, McKenna M, Malkin A and Lyng FM. Raman spectroscopy for cytopathology of exfoliated cervical cells. Faraday Discuss 2016; 187: 187-198.
[38] Talari ACS, Movasaghi Z, Rehman S and Rehman IU. Raman spectroscopy of biological tissues. Applied Spectroscopy Reviews 2015; 50: 46-111.
[39] Ramos IR, Malkin A and Lyng FM. Current advances in the application of Raman spectroscopy for molecular diagnosis of cervical cancer. Biomed Res Int 2015; 2015: 561242.
[40] Wenzel T, Carvajal Berrio DA, Daum R, Reisenauer C, Weltmann KD, Wallwiener D, Brucker SY, Schenke-Layland K, Brauchle EM and Weiss M. Molecular effects and tissue penetration depth of physical plasma in human mucosa analyzed by contact- and marker-independent Raman microspectroscopy. ACS Appl Mater Interfaces 2019; 11: 42885-42895.
[41] Duraipandian S, Traynor D, Kearney P, Martin C, O'Leary JJ and Lyng FM. Raman spectroscopic detection of high-grade cervical cytology: using morphologically normal appearing cells. Sci Rep 2018; 8: 15048.